In conclusion we would like to emphasize that the method itself being a numerical integration of differential equation can be applied for a variety of different problems. We note also that the basic unknown is the highest derivative appearing in the governing differential equation. Hence, the proposed numerical procedure involves numerical integration rather than numerical differentiation (as in case of the finite difference method). It is, therefore, not surprising that the obtained accuracy for the same number of equations is of superior accuracy in comparison with methods based on numerical differentiation.[4]

### References


[1] Vlasov, V. Z., "General Theory of Shells and its Applications in Engineering," N-64-19883, 1964, NASA.

[2] Sanders, J. L., "Nonlinear Theories for Thin Shells," *Quarterly of Applied Mathematics*, Vol. XXI, No. 1, 1963.

[3] Hajdin, N., "A Method for Numerical Solution of Boundary Value Problems," *Translations of the Civil Engineering Department*, Vol. 4, 1958, Belgrade.

[4] Hadid, A., "An Analytical and Experimental Investigation into the Bending Theory of Elastic Conoidal Shells," Dr. Sc. dissertation, 1964, Univ. of Southampton.


# Fundamental Natural Frequencies of Circular Sandwich Plates


JAO-SHIUN KAO*
*Marquette University, Milwaukee, Wis.*
AND
ROBERT J. ROSS†
*U.S. Naval Civil Engineering Laboratory, Port Hueneme, Calif.*


### Introduction

VIBRATIONS of sandwich plates have been treated by many investigators. However, all of these investigations pertain to the analysis of rectangular plates; and, to our knowledge, no investigation of vibration of circular sandwich plates exists to date. A comprehensive literature survey (through 1965) may be found in Ref. 1.

The purpose of this Note is to obtain the fundamental natural frequencies of clamped and simply supported circular sandwich plates. The governing equations are developed by means of a variational theorem. For convenience of practical applications, the results are presented in a graph in terms of nondimensional parameters.

The assumptions made in the present analysis are: 1) the face members are treated as membranes; 2) the face layers may be made of different materials and unequal thickness, however the Poisson's ratio is assumed to be the same; 3) both the core and face layers are considered to be isotropic; and 4) the core is assumed to take only the transverse shear stress.

### Analysis

Consider a circular sandwich plate of radius $a$, core thickness $h_3$, and two facings of thickness $h_1$ and $h_2$. Figure 1 shows a typical element of the sandwich plate. Since the fundamental frequency of vibration is the prime objective, the problem can be reduced to one of rotational symmetry.

The total energy of the entire plate can be separated into the following three parts:

Received June 27, 1969; revision received August 27, 1969.

* Associate Professor of Civil Engineering.

† Civil Engineer.

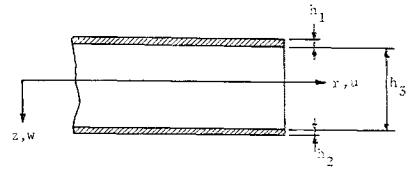


**Fig. 1 Cross section of plate.**

1) The kinetic energy due to the deflection,

$$T = \frac{1}{2} 2\pi \int_0^a \rho w_{,t}^2 dr \tag{1}$$

where $\rho$ is the surface density, $w$ the deflection, and comma denotes differentiation.

2) The strain energy due to displacement of the facings,

$$U_d = \frac{1}{2} 2\pi \sum_{i=1}^{2} \frac{E_i h_i}{(1-\nu^2)} \int_0^a \left(u_{i,r}^2 + \frac{2\nu}{r} u_i u_{i,r} + \frac{1}{r} u_i^2\right) dr \tag{2}$$

where $u_i$ is the displacement at the center of the $i$th face in the radial direction, and $E_i$ and $h_i$ are the elastic modulus and thickness of the $i$th facing, respectively.

3) Strain energy in the core due to shear deformation,

$$U_s = \frac{1}{2} 2\pi G h_3 \int_0^a \left[\frac{u_2 - u_1}{c} + w_{,r}\right]^2 dr \tag{3}$$

where $G$ is the shearing modulus of the core and $c$ is the distance between the middle planes of the facings.

The Lagrangian is then given by

$$L = T - U_d - U_s \tag{4}$$

Taking the variation of $L$, i.e., $\delta L = 0$, leads to the Euler equations

$$-\rho w_{,tt} + G h_3 \left(\frac{\partial}{\partial r} + \frac{1}{r}\right)\left(\frac{u_2 - u_1}{c} + w_{,r}\right) = 0 \tag{5}$$

$$-\frac{E_1 h_1}{(1-\nu^2)}\left[\frac{\nu}{r} u_{1,r} + \frac{1}{r} u_1 - \left(\frac{\partial}{\partial r} + \frac{1}{r}\right)\left(u_{1,r} + \frac{\nu}{r} u_1\right)\right] + \frac{G h_3}{c}\left(\frac{u_2 - u_1}{c} + w_{,r}\right) = 0 \tag{6}$$

$$-\frac{E_2 h_2}{(1-\nu^2)}\left[\frac{\nu}{r} u_{2,r} + \frac{1}{r} u_2 - \left(\frac{\partial}{\partial r} + \frac{1}{r}\right)\left(u_{2,r} + \frac{\nu}{r} u_2\right)\right] - \frac{G h_3}{c}\left(\frac{u_2 - u_1}{c} + w_{,r}\right) = 0 \tag{7}$$

Substituting the resulting equation obtained by differentiating Eq. (5) and dividing by $Gh_3$ into the difference between Eqs. (7) and (6) yields

$$\alpha = \frac{\rho D}{(G h_3)^2} w_{,ttr} - \frac{D}{G h_3} \frac{\partial}{\partial r}\left(\frac{\partial}{\partial r} + \frac{1}{r}\right) w_{,r} - w_{,r} \tag{8}$$

where

$$\alpha = (u_2 - u_1)/c \tag{9a}$$

$$D = E_1 E_2 h_1 h_2 c^2/(1-\nu^2)(E_1 h_1 + E_2 h_2) \tag{9b}$$

Substituting Eq. (8) into the Euler equations reduces Eqs. (5, 6, and 7) to one equation in $w$,

$$\nabla^4 w = -(\rho/D) w_{,tt} + (\rho/G h_3)\nabla^2 w_{,tt} \tag{10}$$

where

$$\nabla^2 = \partial^2/\partial r^2 + (1/r)\partial/\partial r$$
$$\nabla^4 = \nabla^2 \cdot \nabla^2 \tag{11}$$

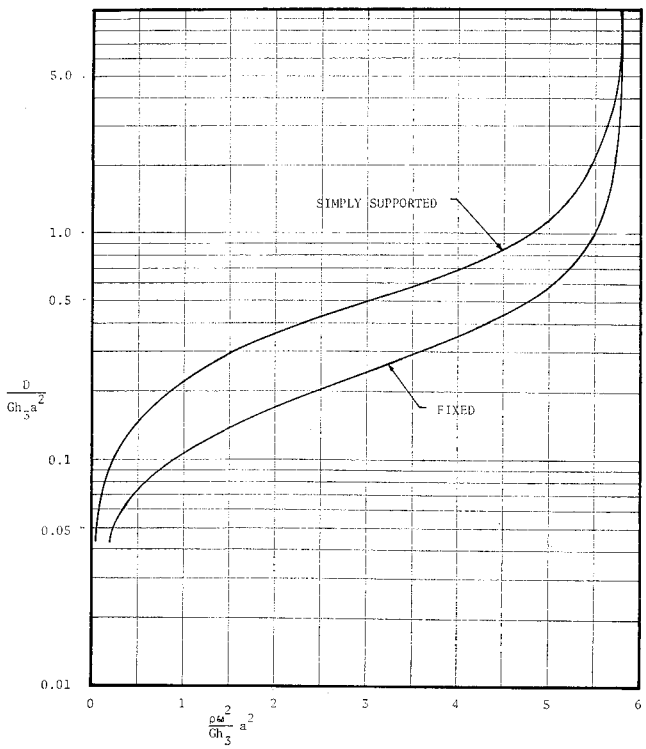


**Fig. 2 Nondimensional frequencies vs rigidity.**

The corresponding boundary conditions at $r = a$ are

$$\alpha + w_{,r} = 0 \text{ or } w = 0 \tag{12a}$$

$$\alpha_{,r} + (\nu/r)\alpha = 0 \text{ or } \alpha = 0 \tag{12b}$$

Assuming a harmonic solution of the form

$$w = Re^{i\omega t} \tag{13}$$

where $R$ is some function of $r$ only, reduces Eq. (10) to

$$[\nabla^2 - \beta_1^2][\nabla^2 + \beta_2^2]R = 0 \tag{14}$$

where

$$\beta_1^2 = -\frac{1}{2}\frac{\rho\omega^2}{Gh_3} + \frac{1}{2}\left[\left(\frac{\rho\omega^2}{Gh_3}\right)^2 + 4\frac{\rho\omega^2}{D}\right]^{1/2} \tag{15a}$$

$$\beta_2^2 = \frac{1}{2}\frac{\rho\omega^2}{Gh_3} + \frac{1}{2}\left[\left(\frac{\rho\omega^2}{Gh_3}\right)^2 + 4\frac{\rho\omega^2}{D}\right]^{1/2} \tag{15b}$$

The general solution of Eq. (14) is

$$R = A_1J_0(\beta_2 r) + A_2Y_0(\beta_2 r) + A_3I_0(\beta_1 r) + A_4K_0(\beta_1 r) \tag{16}$$

where $A_1$ through $A_4$ are arbitrary constants and $J_0$, $Y_0$, $I_0$, and $K_0$ are, respectively, the Bessel Functions of the first and second kind and the Modified Bessel Functions of the first and second kind of order zero. Since $Y_0$ and $K_0$ are singular at $r = 0$,

$$A_2 = A_4 = 0 \tag{17}$$

The characteristic equation can be obtained by considering the specific boundary conditions. First consider a clamped supported. The boundary conditions at $r = a$ are

$$w = 0 \text{ and } \alpha = 0 \tag{18}$$

Applying Eqs. (18) evaluated at $r = a$ to Eq. (16), using the Recurrnce Formulas for the derivates of the Bessel Functions, and setting the determinant of the coefficients on $A_1$ and $A_3$ to zero yields the characteristic equation

$$I_0(\lambda_1)\left[\lambda_2^3J_3(\lambda_2) - 4\lambda_2^2J_2(\lambda_2) + \left(\frac{\lambda_1^4 - \lambda_1^2\lambda_2^2 + \lambda_2^4}{\lambda_2^2 - \lambda_1^2}\right)\lambda_2J_1(\lambda_2)\right] + J_0(\lambda_2)\left[\lambda_1^3I_3(\lambda_1) + 4\lambda_1^2I_2(\lambda_2) + \left(\frac{\lambda_1^4 - \lambda_1^2\lambda_2^2 + \lambda_2^4}{\lambda_2^2 - \lambda_1^2}\right)\lambda_1I_1(\lambda_1)\right] = 0 \tag{19}$$

where

$$\lambda_1 = a\beta_1 \tag{20a}$$

$$\lambda_2 = a\beta_2 \tag{20b}$$

It should be noted that $\lambda_1$ and $\lambda_2$ are dimensionless parameters. The relationships between $\lambda_1$ and $\lambda_2$ are

$$\lambda_2^2 - \lambda_1^2 = (\rho\omega^2/Gh_3)a^2 \tag{21a}$$

$$\frac{(\lambda_1^2 + \lambda_2^2)^2 - (\lambda_2^2 - \lambda_1^2)^2}{4(\lambda_2^2 - \lambda_1^2)} = \frac{Gh_3}{D}a^2 \tag{21b}$$

$$\frac{\lambda_1^4 - \lambda_1^2\lambda_2^2 + \lambda_2^4}{\lambda_2^2 - \lambda_1^2} = \left(\frac{\rho\omega^2}{Gh_3} + \frac{Gh_3}{D}\right)a^2 \tag{21c}$$

Thus by knowing the physical constants of the sandwich plate, it is possible to solve for the frequency once $\lambda_1$ and $\lambda_2$ are known.

Next consider a simply supported sandwich plate. The boundary conditions at $r = a$ are

$$w = 0 \text{ and } \alpha_{,r} + (\nu/r)\alpha = 0 \tag{22}$$

Using the same procedure as outlined for the clamped condition leads to the characteristic equation

$$I_0(\lambda_1)\left[-\lambda_2^4J_4(\lambda_2) + (7+\nu)\lambda_2^3J_3(\lambda_2) - 4(1+\nu)\lambda_2^2J_2(\lambda_2) - \left(\frac{\lambda_1^4 - \lambda_1^2\lambda_2^2 + \lambda_2^4}{\lambda_2^2 - \lambda_1^2}\right)\times\left(\lambda_2^2J_2(\lambda_2) - (1+\nu)\lambda_2J_1(\lambda_2)\right)\right] + J_0(\lambda_2)\left[\lambda_1^4I_4(\lambda_1) + (7+\nu)\lambda_1^3I_3(\lambda_1) + 4(1+\nu)\lambda_1^2I_2(\lambda_1) + \left(\frac{\lambda_1^4 - \lambda_1^2\lambda_2^2 + \lambda_2^4}{\lambda_2^2 - \lambda_1^2}\right)\times\left(\lambda_1^2I_2(\lambda_1) + (1+\nu)\lambda_1I_1(\lambda_1)\right)\right] = 0 \tag{23}$$

## Results and Conclusions

The fundamental frequency is obtained for the smallest positive roots of the characteristic equations. Figure 2 shows the plot of $\lambda_2^2 - \lambda_1^2$ and

$$\frac{4(\lambda_2^2 - \lambda_1^2)}{(\lambda_1^2 + \lambda_2^2)^2 - (\lambda_2^2 - \lambda_1^2)^2}$$

i.e., Eq. (21a) plotted as the abscissa and the reciprocal of Eq. (21b) plotted as the ordinate and using $\nu = 0.3$. It should be noted that when Eq. (21b) equals zero the shear rigidity is infinite and thus the frequency obtained is for a single-layer isotropic circular plate without shear deformation. The numerical results obtained for this special case agree with those obtained by Pandalai and Patel[2] for the isotropic plate. When Eq. (21b) becomes very large, the

deformation is entirely due to shear. Thus the two plots coincide for large shear deformation, as they should.

### References

[1] Habip, L. M., "A Survey of Modern Developments in the Analysis of Sandwich Structures," *Applied Mechanics Reviews*, Vol. 18, No. 2, 1965, p. 93.

[2] Pandalai, K. A. and Patel, S. A., "Natural Frequencies of Orthotropic Circular Plates," *AIAA Journal*, Vol. 3, No. 4, April 1965, pp. 780–781.

# Effect of Varying Wall Temperature and Total Temperature on Transition Reynolds Number at Mach 6.8

DAL V. MADDALON*
*NASA Langley Research Center, Hampton, Va.*

### Nomenclature

$M$ = Mach number
$P$ = pressure, psia
$\dot{q}$ = heating rate
$R$ = Reynolds number
$T$ = temperature, °R
$V$ = velocity, fps
$x$ = longitudinal distance from model leading edge, in.
$\delta$ = boundary-layer thickness, in.

***Subscripts***

$aw$ = adiabatic wall conditions (turbulent flow)
$e$ = boundary-layer edge conditions
$o$ = stagnation conditions
$t$ = beginning of transition
tun = tunnel wall temperature
$T$ = beginning of turbulent flow (peak heating point)
$w$ = model wall temperature
$\infty$ = freestream conditions

***Superscripts***

$\sim$ = root mean square

### Introduction

At hypersonic speeds there is much confusion regarding the trend of transition Reynolds number with wall-to-total-temperature ratio.[1–4] An investigation of this effect was therefore undertaken at $M_e \approx 6.8$ over a comparatively large range of wall-to-total-temperature ratio in the Langley $M_\infty \approx 20$ 22-in. helium tunnel. To obtain different levels of $T_w/T_o$, investigators using conventional wind tunnels generally vary model wall temperature,[2] whereas investigators using facilities such as shock tunnels and ranges[3,4] generally vary stagnation temperature. In the present study, both $T_w$ and $T_o$ were varied while holding Mach number, Reynolds number, and $T_w/T_o$ constant. This was done because it was thought that wall cooling might stabilize the boundary layer, whereas changing total temperature might prove destabilizing by altering the facility's disturbance level. Wagner et al.,[5] have shown that in unheated flow the freestream disturbance level in the 22-in. facility is a result only of sound radiation from the turbulent nozzle wall boundary layer; however, heating the flow could alter the tunnel's noise level and or introduce additional disturbance modes such as temperature spottiness. The helium wind tunnel is unique in this ability to operate at $M_\infty \approx 20$ utilizing both heated and unheated flow.

### Test Facility, Model, and Techniques

Experiments were conducted in the Langley $M_\infty \approx 20$ hypersonic helium tunnel. This tunnel has a contoured nozzle and a 22-in.-diam test section. For the present investigation, the model was supported from a floor mount. The freestream Mach number in the test core, though constant at any given stagnation pressure, varied with stagnation pressure from a low of 20.1 at 1015 psia to 21.4 at 2515 psia. A calibration and description of the facility is given in Ref. 6. The local inviscid Mach numbers specified in this study were verified experimentally by static pressure and Pitot pressure measurements at the boundary-layer edge. Test conditions are summarized in Table 1, which includes the freestream disturbance levels measured by Wagner[5] with a hot wire anemometer in unheated flow (attempts in that study to repeat the hot wire measurements in heated flow were unsuccessful because of repeated wire failures).

The transition model was a sharp leading edge (0.002 in. thick), smooth, flat plate 21 in. long and 14 in. wide. The plate was set at 10° angle of attack; the local Mach number was therefore about 6.8. The model was fabricated of AISI 405 stainless steel with a wall thickness of about 0.030 in. and had swept end plates. This was the same model used in Cary's study[2] and a more complete model description can be found in this reference. Thirty-four thermocouples placed along the model centerline and spaced about 0.5 in. apart were used to determine heating rates and, thence, transition location. The rate of surface temperature rise was obtained from a second-degree curve fit (by the method of least squares) to the temperature time data for a 0.5-sec time interval starting about 2 sec after flow was established. The length of the run was about 6 sec. Conduction errors were checked and found to be negligible. The beginning of transition $(R_{e,x})_t$ was defined as the point where the $\dot{q}$ vs $R_{e,x}$ curve departed from a laminar $\frac{1}{2}$ power slope, whereas the beginning of turbulent flow (end of transition) $(R_{e,x})_T$ was taken as the peak heating point.

To avoid the problem of frost formation on the model's surface, a 0.002-in.-thick Mylar sheet was placed over the entire surface of the model such that no air gaps existed between the surface and the Mylar sheet. The tunnel was then evacuated to a pressure of about 0.2 mm Hg, and the model internally cooled with liquid nitrogen to the desired wall temperature (generally uniform within ±10°R). The gaseous nitrogen was re-routed out of the tunnel and exhausted to the atmosphere. A frost coating estimated at about 0.002-in. thickness formed on top of the Mylar cover when the wall was cooled below 360°R. Immediately before flow was established, the cover was rapidly removed and the run started. This procedure enabled runs to be made with the model completely frost free.

### Results

The effect of wall cooling on transition Reynolds number is presented in Fig. 1 for two unit Reynolds numbers where, for a given unit Reynolds number and total temperature, the freestream disturbance level is constant (model wall temperature was independently varied). For unheated flow the measured disturbance levels of Ref. 5 are included in Table 1. Considering first the data obtained in unheated flow (open symbols), both $(R_{e,x})_t$ and $(R_{e,x})_T$ are seen to decrease continuously from $T_w/T_o \approx 0.3$ to $T_w/T_o \approx 0.8$ with no transition reversal evident within this wall-to-total-temperature ratio range. This is the same trend observed by Cary.[2] A further increase past the adiabatic wall temperature ratio to $T_w/T_o \approx 0.95$, however, results in a pronounced increase in the transition location. In this case the plate is transferring heat to the flow. The sharp increase

Received August 15, 1969.

* Aerospace Engineer, Flow Analysis Section.